Dispersion of surface elastic waves on Z-$LiNbO_3$ films on Z-sapphire

Léa La Spina,[1] Quentin Micard,[1,2] Alexis Mosset,[3] Samuel Margueron,[4] Ausrine Bartasyte,[1] and Vincent Laude[3,*]

[1]*Université de Franche-Comté, CNRS, institut FEMTO-ST, 26 rue de l'Epitaphe, 25000 Besançon, France*
[2]*Annealsys, 139 Rue des Walkyries, 34000 Montpellier, France*
[3]*Université de Franche-Comté, CNRS, institut FEMTO-ST, 15B avenue des Montboucons, 25000 Besançon, France*
[4]*SUPMICROTECH, CNRS, institut FEMTO-ST, 26 rue de l'Epitaphe, 25000 Besançon, France*

Epitaxial thin films of lithium niobate with a thickness of 160 nm, oriented along the cristallographic c-axis, were grown by direct liquid injection chemical vapor deposition on c-sapphire substrates. Different families of very high-frequency surface acoustic waves with general polarization exist in such piezoelectric films on high-velocity substrates. Surface Brillouin light scattering measurements, complemented with fast finite element analysis of wave dispersion, demonstrate Rayleigh, leaky shear and leaky longitudinal surface waves, excited at frequencies between 10 and 30 GHz. The Brillouin technique reveals dispersion and anisotropy of propagation without the implementation of high-frequency surface acoustic wave transducers.

Surface acoustic wave (SAW) micro-resonators, based on bulk lithium niobate (LN) or lithium tantalate, typically operate up to frequencies of 3.7 GHz [1]. An alternative technology, however, is needed for high-frequency 5G filters. Indeed, the frequency of SAW devices is mainly proportional to the phase velocity of the acoustic wave in the material and inversely proportional to the period of interdigital transducers (IDT). IDT period miniaturization is getting close to a practical limit, mostly due to the cost of equipment needed to obtain a finer resolution and the stability of IDTs operated at high power density. An alternative way to achieve higher frequencies is to use piezoelectric thin films on high velocity substrates. Acoustic waves in the substrate must be faster than in the thin film so that the film acts as a waveguide, and thus that surface acoustic waves are confined and accelerated in the piezoelectric film [2]. The thinner the piezoelectric layer, the faster the velocity of the confined wave. For instance, the Rayleigh SAW velocity on (ZX) LN (crystal orientation and SAW propagation direction are indicated in IEEE Std-176 convention [3], Z-LN) is 3730 m/s, whereas it is 5555 m/s on c-sapphire (Z-sapphire, where crystallographic c-orientation stands for the (ZX) orientation). For the 160-nm-thick layer of Z-LN on Z-sapphire considered in this work, the velocities of guided elastic waves with wavelength of 1 µm are typically around 5400 m/s [4].

LN is often used in SAW devices in the form of bulk single crystals, or of thin films obtained by the bonding/ion-slicing process, bonding/polishing or epitaxial growth [4–7]. On the one hand, the top-down fabrication of single-crystal LN thin films implies a polishing step limiting reproducibility and homogeneity of the thickness across the wafer, which is a critical parameter for dispersive waves. Additionally, in the case of the ion-slicing technique, the film thickness is limited to the range from $\approx$ 300 nm to 1 µm, while it is difficult to attain films with well controlled thickness below a 1 µm thickness by means of bonding/polishing. On the other hand, epitaxy techniques allow one to reach thicknesses smaller than 300 nm. LN thin films can be grown epitaxially by different techniques [8], such as for example pulsed laser deposition (PLD) [9, 10], sol-gel [11], RF-sputtering [12] and metal-organic chemical vapor deposition (MOCVD) [4, 13]. However, the synthesis of high-quality LN films with physical properties comparable to the ones of single crystals is not an easy task and particular attention must be paid to composition/nonstoichiometry of the layer (controlled Li nonstoichiometry LN and absence of parasitic phases) [8, 14], single in-plane and out-of-plane orientations, ferroelectric domain structure, and smoothness of the surface. Compared with other techniques, MOCVD allows for an easier control of composition. High quality LN epitaxial films with a pure LN phase and controlled nonstoichiometry were grown by pulsed-injection MOCVD and high performance of 5.3 GHz SAW devices based on these films was demonstrated [4].

Bulk acoustic waves [15, 16] and Rayleigh waves [17] in single crystals of LN have already been widely investigated by Brillouin Light Scattering (BLS). However, experimental data regarding surface BLS on deposited LN thin films are lacking. The goal of this work is to identify, measure and compare the various surface acoustic waves appearing in a piezoelectric epitaxial Z-LN thin film on a high-velocity Z-sapphire substrate, by means of surface BLS measurements. The latter indeed allow us to detect thermally-generated guided acoustic waves, or surface phonons, and to evaluate their velocities [18]. The observed surface phonon frequencies are in the range of 10 to 30 GHz in our experiment. The dispersion and the polarization of leaky surface acoustic waves on an arbitrary multilayer are obtained by calculating their dispersion relation relating angular frequency ω and wavevector k. Obtaining the dispersion relation is fairly easy in a finite-dimensional problem but is more difficult in the case of infinite domains. Here, we approximate the problem with a perfectly matched layer (PML) [19] to account for radiation inside the semi-infinite substrate. Combined with wave finite element analysis, the dispersion relation of leaky surface waves is obtained, including their radiation loss [20]. The surface guided acoustic waves are detected by surface BLS and are in a good agreement with the results of the finite element model.

The 160-nm-thick Z-LN thin film on a Z-sapphire substrate was deposited by means of direct liquid injection chemical va-

* vincent.laude@femto-st.fr

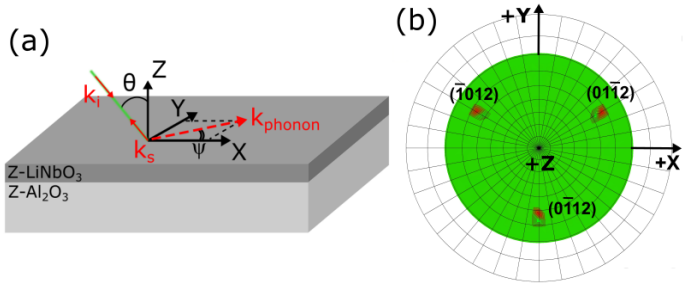

FIG. 1. Experimental setup. (a) The LN thin film is grown on a sapphire substrate. The (X,Y,Z) orthogonal frame is used for both experiment framework and numerical simulation. With respect to the hexagonal crystallographic unit cell, Z is parallel to the c-axis and X is parallel to the a-axis. θ is the angle of incidence of the laser in the surface Brillouin light scattering experiment and ψ is the in-plane angle of the phonon wavevector k_{phonon}. k_i and k_s are respectively the incident and backscattered optical wavevectors. (b) X-ray diffraction pole figure of <01$\bar{1}$2> family planes of the Z-LN thin film on a Z-sapphire substrate.

por deposition (DLI-CVD, *Annealsys MC-100* reactor) (Fig. 1a, more details about deposition conditions can be found in Ref. [14]). The thin film stoichiometry, residual stresses and orientation were studied by means of Raman spectroscopy and X-ray diffraction (XRD, using Cu K_α radiation). According to XRD and Raman data, the film contained 48.8 mol% of Li_2O (close to the composition (48.34 mol%) of congruent LN crystal) and the film was under 1 GPa of tensile residual biaxial stress in the substrate plane (more details on the estimation of residual stresses and nonstoichiometry of LN films can be found in Ref. [14]). The effects of nonstoichiometry and residual stresses were neglected in BLS analysis and numerical simulations. A X-ray diffraction (XRD) pole figure of $\{01\bar{1}2\}$ family planes (at diffraction angle $2\theta_{\text{diff}} = 23.6°$) was measured to assess the in-plane orientation of the film (see also the supplemental material for a $\theta/2\theta$ XRD pattern and a rocking curve measurement for (0006) reflections). The three reflections of the $\{01\bar{1}2\}$ plane family, spaced by 120°, were visible at tilt angle $\chi_{\text{diff}} = 57.3°$, indicating single orientation of the LN film in the substrate plane (Fig. 1b). Note that angles $2\theta_{\text{diff}}$ and χ_{diff} only refer to the X-ray diffraction measurement and should not be confused with the angles defined in Fig. 1a for BLS. In the literature, epitaxy of Z-LN on Z-sapphire was mainly reported with two in-plane orientations rotated by 60° in the substrate plane (represented by six reflections of $\{01\bar{1}2\}$ family in pole figure). The single-crystalline quality of films (single orientation of the film, identical to that of the substrate) allowed us for selection of the proper direction for phonon propagation during surface BLS measurements.

The BLS spectra in Fig. 2a were obtained in the backscattering configuration, using a 200 mW p-p polarized light beam (single longitudinal mode of the $\lambda = 532$ nm line of a diode-pumped solid-state laser) focused to a spot of a few microns. The laser beam was focused on the sample surface and the backscattered light was collected though a x20 microscope objective. Brillouin frequency shifts were measured using a Sandercock-type, (3+3) pass, tandem Fabry-Perot interferometer [21]. As both substrate and film are transparent, the collecting time ranged from 6 to 8 hours. As Fig. 1a depicts, the laser beam is incident on the sample with an angle θ, resulting in a surface phonon wavenumber $k = 4\pi\sin(\theta)/\lambda$. For a Z-LN film supported by a Z-sapphire substrate, the shear bulk wave velocity in the film is lower than in the substrate. Since the film thickness is deeply submicrometric, the velocity of surface guided waves is hence expected to appear between the film Rayleigh wave (RW) and the substrate shear wave velocity. Above this limit, observable surface guided modes are leaky, radiating energy in the substrate [22].

The measured frequency shifts, due to inelastic light scattering on the surfaces of the film, are reported in Fig. 2a for different values of the incidence angle θ. Frequencies were extracted using the damped harmonic oscillator (DHO) fitting procedure (for each peak independently) of the *GHOST software* and measurement uncertainties were estimated from the FWHM of the fitted peaks [23]. Optics aperture and misalignment are the main causes of peak broadening and asymmetry, especially for small θ where the uncertainty is the greatest [24]. The Brillouin frequency shifts vary depending on the wavenumber, i.e. on the incident angle θ, thus confirming the surface-guided nature of the observed acoustic waves [25]. Here, three surface acoustic waves appear. For $\theta = 80°$, the slowest and more intense response (for a frequency shift around 15 GHz), is from the Rayleigh wave (RW), whereas the other two responses are attributed to a leaky shear SAW (LSSAW) around 20 GHz and a leaky longitudinal SAW (LLSAW) around 30 GHz [4]. For comparison, in the backscattering configuration the Brillouin peaks for bulk phonons would appear above 31 GHz for Z-LN and above 40 GHz for Z-Sapphire.

Very often, acoustic wave dispersion in multilayers is obtained using a plane-wave approach and matrix algebra [26–28]. There is then an implied assumption that all layers are homogeneous, excluding the possibility of material composition gradients or of inhomogeneities. Furthermore, elaborated Green's function coupling problems with finite element analysis must be solved when a spatial structuration at the surface of the multilayer is taken into account. Hence, we chose to perform numerical simulations using a finite element method (FEM) for open, radiating systems [20]. Invariance along the x- and y-axes is assumed, thus we represent the problem by a line mesh in 3D space, to account for an arbitrary solution varying along the z-axis. Material tensors are rotated beforehand depending on the orientation selected. The 1D mesh, on which solutions are calculated, is divided into finite elements. All possible elastic waves are generated thanks to a stochastic (i.e. random) excitation limited to the LN layer. A perfectly matched layer (PML) is added at the bottom of the stack, to account for the semi-infinite substrate. In this artificial absorbing layer, wave amplitudes decrease exponentially until they can be neglected so that reflections at the bottom of the substrate, that could disturb the calculation, are avoided. The elastodynamic equation, describing elastic wave propagation,

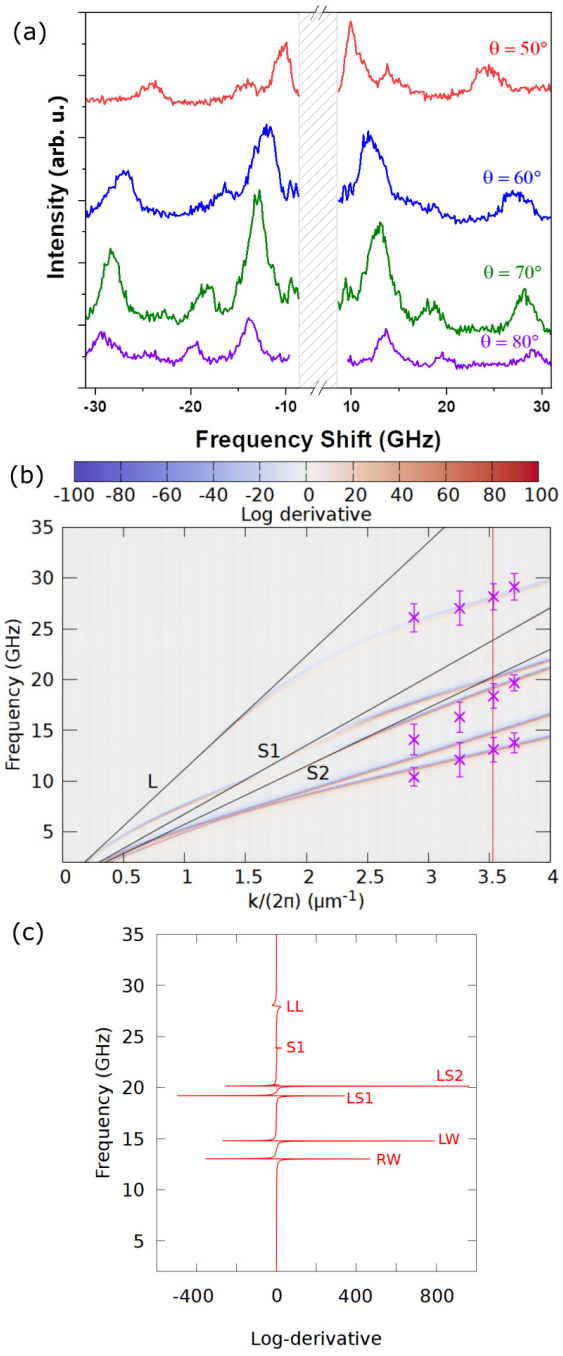

FIG. 2. (a) Surface Brillouin Light Scattering spectra of the 160-nm-thick Z-LN thin film on Z-sapphire, for 4 different values of the incidence angle, θ. (b) The log-derivative of the response obtained from the stochastic FEM simulation is plotted as a function of wavenumber and frequency. Purple crosses indicate the experimental points determined from BLS spectra (presented in (a)). Black lines are for the bulk longitudinal (L) and shear (S1, S2) waves of the sapphire substrate. A cut of the log-derivative of the response is shown in (c) at the fixed wavenumber $k/2\pi = 3.53\ \mu m^{-1}$. Labels RW, LW, LS1, LS2, and LL stand for Rayleigh, Love, Leaky shear, and Leaky longitudinal waves, respectively.

TABLE I. Calculated relative polarization of the waves identified in Fig. 2b.

Polarization	p_x	p_y	p_z
1st band (RW)	0.12	0.08	0.80
2nd band (LW)	0.02	0.94	0.04
3rd band (LS1)	0.16	0.78	0.06
4th band (LS2)	0.52	0.25	0.23
5th band (LL)	0.60	0.04	0.36

is

$$-\nabla.T + \rho\frac{\partial^2\mathbf{u}}{\partial t^2} = \mathbf{f} \tag{1}$$

with T the stress tensor, $\mathbf{u}$ the displacement vector, and $\mathbf{f}$ an applied body force. Taking piezoelectricity into account implies considering in addition Poisson's equation, describing the charge distribution

$$-\nabla.\mathbf{D} = 0 \tag{2}$$

with $\mathbf{D}$ the electric displacement vector. The constitutive relations of piezoelectricity are

$$T_{ij} = c_{ijkl}S_{kl}(\mathbf{u}) - e_{kij}E_k, \tag{3}$$
$$D_i = e_{ikl}S_{kl}(\mathbf{u}) + \varepsilon_{ij}E_j, \tag{4}$$

where c, e, ε and S are respectively the elastic, piezoelectric, dielectric and strain tensors and $\mathbf{E} = -\nabla\phi$ is the electric vector deriving from a scalar electric potential ϕ. All vectors and tensors appearing above are then represented as finite element functions defined on the mesh. Note that all fields include an implicit plane wave dependence $\exp(-\imath\mathbf{k}\cdot\mathbf{r})$ with $\mathbf{k}$ the wavevector along the surface of the multilayer. Hence $E_j = -\frac{\partial\phi}{\partial x_j} + \imath k_j\phi$ and $S_{ij}(\mathbf{u}) = \frac{1}{2}(\frac{\partial u_i}{\partial x_j} - \imath k_j u_i + \frac{\partial u_j}{\partial x_i} - \imath k_i u_j)$, for instance. Further details about the method employed are given in Ref. [20].

The formulation above was used to obtain dispersion maps for surface guided elastic waves as follows. The calculation is performed for a definite frequency ω and wave vector k pair. The energy response to a random excitation of the top layer is obtained as a function $E(\omega,k)$, similar to a density of states. The stochastic response for waves propagating in a 160 nm Z-LN film deposited on a Z-oriented sapphire substrate is shown in Fig. 2b. The simulation is performed for waves propagating along the x-axis. A cross-section at the fixed wavenumber $k/2\pi = 3.53\ \mu m^{-1}$ is further presented in Fig. 2c.

A total of five bands for surface guided waves are apparent in Fig. 2b; they generally have a damped Lorentzian shape as a function of frequency. The lowest three waves whose dispersion appear under the bulk shear waves of sapphire are guided in the LN thin film and evanescent in the substrate (labels RW, LW and LS1 in Fig. 2c). The fourth surface band (label LS2 in Fig. 2c) crosses the bulk shear bands of sapphire (S1 and S2) for some values of k and thus switches from a leaky guided wave to a surface guided wave. The fifth surface band (label LL in Fig. 2c) is always above the bulk shear

bands of sapphire and is thus identified as a leaky guided wave that is partially confined in the Z-LN thin film but radiates in the substrate. The relative polarization of these waves was determined from the numerical response, to confirm their nature (see Table I). The first and fifth bands, i.e. the slowest and fastest waves, have a mostly sagittal polarization and are respectively identified as a Rayleigh wave (RW) and a Sezawa wave (LL). The second and third bands have a dominant y-oriented polarization, thus corresponding to shear waves and are identified as Love waves (LW and LS1). Lastly, the fourth band (LS2) presents polarization components in all x, y and z directions, and the relative polarization changes as it switches from a leaky guided wave to a surface guided wave.

The experimentally determined phonon frequencies reported on the dispersion diagram of Fig. 2b agree reasonably well with numerical simulations. Two of the surface waves appearing in the dispersion diagram, however, are not observed in the BLS measurements. Actually, pure horizontal shear waves (Love type wave) are not observed by surface BLS, because depolarized scattering (p-s) from the LW is much less intense than from the other modes [18]. The third (LS1) and fourth (LS2) peaks may be too close to be separable in the measurements. The BLS measurements for the Rayleigh wave and the leaky longitudinal SAW agree well with their expected dispersion, whereas for the leaky shear SAW frequencies are a bit off. Indeed, the intensity of the LSSAW peak is much lower compared to the other peaks, rendering the estimation of frequency shifts less precise because of the frequency-dependent pedestal of the RW peak. Furthermore, imperfections resulting from phonon loss in the LN film, the impact of roughness on surface wave propagation, and the influence of grain boundaries on effective elastic properties are difficult to evaluate and were not taken into account in numerical computations (see the supplemental material for surface roughness measurements).

Finally, Fig. 3 presents the dispersion for a fixed wavenumber ($k/2\pi = 3.53\,\mu m^{-1}$ or $\theta = 70°$) and a variable angle ψ in the (x,y) plane. This map illustrates the anisotropy of propagation of surface guided waves. The five numerical surface bands appearing are those observed in Fig. 2(b) at high frequencies and wavenumbers. As expected for a Z-LN orientation, the frequency variations of phase velocity remain small. Surface BLS measurements (purple crosses) have been added to Fig. 3 for a fixed incidence angle $\theta = 70°$ and in-plane rotation angles $\psi = 0°, 5°, 25°, 30°, 45°, 60°$ and $90°$. We clearly observe the Brillouin responses for the Rayleigh wave (around 13 GHz), the leaky shear (around 18 GHz), and the leaky longitudinal SAW (around 28 GHz). Overall, measurements are in fair agreement with numerical simulations.

In summary, we have explored the guided phonons, or guided elastic waves, that propagate on the surface of a Z-LN/Z-sapphire heterostructure in the range from 10 to 30 GHz. Surface phonon frequencies were determined by means of surface Brillouin light scattering with a varying angle of incidence and in-plane angle. Surface phonon dispersion and polarization were obtained numerically combining finite element analysis and a stochastic excitation method [20]. Experimental and numerical dispersion of Brillouin responsive surface phonons agree rather well. Deviations are assumed to result mainly from a detection limitation for certain phonon polarizations with the set-up used and from low surface BLS efficiency.

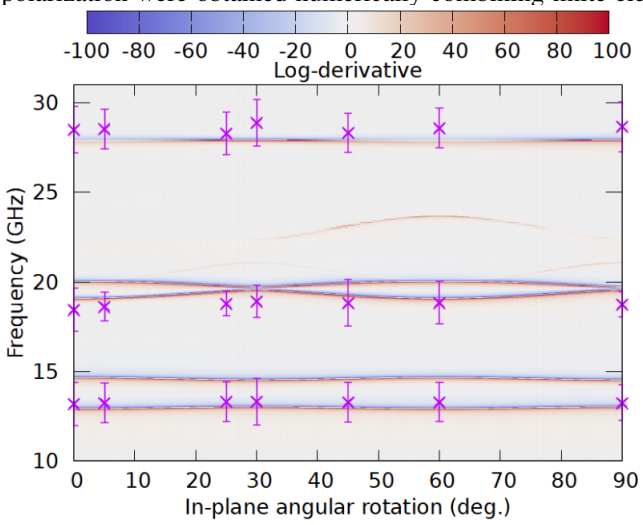

FIG. 3. In-plane dispersion of elastic waves in the thin film Z-LN on Z-Sapphire at a fixed wavenumber $k/2\pi = 3.53\,\mu m^{-1}$. Angles $0°$ and $90°$ correspond to propagation along the x-axis and the y-axis, respectively. Purple crosses are the surface BLS measurements (performed at $\theta = 70°$).

SUPPLEMENTARY MATERIAL

See supplementary material for additional X-ray diffraction and atomic force microscopy measurements.

ACKNOWLEDGMENTS

The authors are grateful to the French National Research Agency for funding through grants ANR MAXSAW Grant No. ANR-20-CE24-0025 and ANR LINKS Grant No. ANR-20-CE08-0025, and to the EUR EIPHI program Grant No. ANR-17-EURE-0002. We thank Virginie Moutarlier at UTINAM Institute for support in using X-ray diffractometer. This work was partly supported by the French RENATECH network and its FEMTO-ST technological facility.

DATA AVAILABILITY STATEMENT

The data that support the findings of this study are available from the corresponding author upon reasonable request.

[1] T. Kimura, M. Omura, Y. Kishimoto, and K.-Y. Hashimoto, in *2018 IEEE/MTT-S International Microwave Symposium-IMS* (IEEE, 2018) pp. 846–848.

[2] E. Dieulesaint and D. Royer, *Ondes élastiques dans les solides - Tome 1: Propagation libre et guidée* (Masson, Paris, 1996).

[3] A. Meitzler, D. Berlincourt, G. Coquin, F. Welsh III, H. Tiersten, and A. Warner, *IEEE Standard on Piezoelectricity, ANSI/IEEE Standard Series-176* (Institute of Electrical and Electronics Engineers, New York, USA, 1978).

[4] A. Almirall, S. Oliveri, W. Daniau, S. Margueron, T. Baron, P. Boulet, S. Ballandras, S. Chamaly, and A. Bartasyte, Applied Physics Letters **114**, 162905 (2019).

[5] H. Xu, S. Dong, W. Xuan, U. Farooq, S. Huang, M. Li, T. Wu, H. Jin, X. Wang, and J. Luo, Applied Physics Letters **112**, 093502 (2018).

[6] J. Zheng, J. Zhou, P. Zeng, Y. Liu, Y. Shen, W. Yao, Z. Chen, J. Wu, S. Xiong, Y. Chen, X. Shi, J. Liu, Y. Fu, and H. Duan, Applied Physics Letters **116**, 123502 (2020).

[7] S. Zhang, R. Lu, H. Zhou, S. Link, Y. Yang, Z. Li, K. Huang, X. Ou, and S. Gong, IEEE Transactions on Microwave Theory and Techniques **68**, 3653 (2020).

[8] A. Bartasyte, S. Margueron, T. Baron, S. Oliveri, and P. Boulet, Advanced Materials Interfaces **4**, 1600998 (2017).

[9] S. Kilburger, R. Chety, E. Millon, P. Di Bin, C. Di Bin, A. Boulle, and R. Guinebretière, Applied surface science **253**, 8263 (2007).

[10] H. Lam, J. Dai, and H. Chan, Journal of crystal growth **268**, 144 (2004).

[11] M. Takahashi, R. Otowa, H. Mori, S. Sato, A. Nishiwaki, K. Wakita, N. Ohnishi, T. Yagi, and T. Uchida, Journal of Applied Physics **96**, 6569 (2004).

[12] N. Fujimura, M. Kakinoki, H. Tsuboi, and T. Ito, Journal of Applied Physics **75**, 2169 (1994).

[13] M. Kadota, T. Ogami, K. Yamamoto, Y. Negoro, and H. Tochishita, Japanese Journal of Applied Physics **48**, 07GG08 (2009).

[14] A. Bartasyte, V. Plausinaitiene, A. Abrutis, T. Murauskas, P. Boulet, S. Margueron, J. Gleize, S. Robert, V. Kubilius, and Z. Saltyte, Applied Physics Letters **101**, 122902 (2012).

[15] T. Błachowicz, Optics Communications **210**, 213 (2002).

[16] R. J. O'Brien, G. J. Rosasco, and A. Weber, in *Light Scattering Spectra of Solids*, edited by G. B. Wright (Springer Berlin Heidelberg, Berlin, Heidelberg, 1969) pp. 623–630.

[17] H. Lim, J. Huang, V. Zhang, M. Kuok, and S. Ng, Journal of Applied Physics **93**, 9703 (2003).

[18] G. Carlotti, Applied Sciences **8**, 124 (2018).

[19] J.-P. Berenger, Journal of computational physics **114**, 185 (1994).

[20] V. Laude and M. E. Korotyaeva, Physical Review B **97**, 224110 (2018).

[21] J. R. Sandercock, "Trends in Brillouin scattering: Studies of opaque materials, supported films, and central modes," in *Light Scattering in Solids III: Recent Results*, edited by M. Cardona and G. Güntherodt (Springer Berlin Heidelberg, Berlin, Heidelberg, 1982) pp. 173–206.

[22] G. Farnell and E. Adler, "Elastic wave propagation in thin layers," in *Physical Acoustics*, Vol. 9 (Elsevier, 1972) p. 35–127.

[23] D. Fioretto and F. Scarponi, Materials Science and Engineering: A **521-522**, 243 (2009), 15th International Conference on Internal Friction and Mechanical Spectroscopy.

[24] C. Flannery and H. von Kiedrowski, Ultrasonics **40**, 83 (2002).

[25] P. Djemia, "La diffusion Brillouin pour caractériser les propriétés élastiques ou magnétiques de multicouches," in *Instrumentation, Mesure, Métrologie - Les ondes en instrumentation* (Lavoisier, Paris, 2009) pp. 11–35.

[26] A. Fahmy and E. Adler, Applied Physics Letters **22**, 495 (1973).

[27] T. Pastureaud, V. Laude, and S. Ballandras, Applied Physics Letters **80**, 2544 (2002).

[28] A. Reinhardt, T. Pastureaud, S. Ballandras, and V. Laude, Journal of Applied Physics **94**, 6923 (2003).